Journal of Quantitative Spectroscopy & Radiative Transfer 214 (2018) 133–145

Contents lists available at ScienceDirect

Journal of Quantitative Spectroscopy & Radiative Transfer

journal homepage: www.elsevier.com/locate/jqsrt

A simplified model of all-sky artificial sky glow derived from VIIRS Day/Night band data

Dan M. Duriscoe[a], Sharolyn J. Anderson[b,*], Christian B. Luginbuhl[c], Kimberly E. Baugh[d]

[a] U.S. National Park Service Night Skies Program (retired), Big Pine, CA, USA
[b] National Park Service, Natural Sounds and Night Skies, Fort Collins, CO, USA
[c] Dark Sky Partners LLC, Tucson, AZ, USA
[d] University of Colorado- CIRES, Boulder, CO, USA

ARTICLE INFO

Article history:
Received 15 November 2017
Revised 25 April 2018
Accepted 25 April 2018
Available online 26 April 2018

Keywords:
Night sky brightness
Light pollution
Landscape scale assessments

ABSTRACT

We present a simplified method using geographic analysis tools to predict the average artificial luminance over the hemisphere of the night sky, expressed as a ratio to the natural condition. The VIIRS Day/Night Band upward radiance data from the Suomi NPP orbiting satellite was used for input to the model. The method is based upon a relation between sky glow brightness and the distance from the observer to the source of upward radiance. This relationship was developed using a Garstang radiative transfer model with Day/Night Band data as input, then refined and calibrated with ground-based all-sky V-band photometric data taken under cloudless and low atmospheric aerosol conditions. An excellent correlation was found between observed sky quality and the predicted values from the remotely sensed data. Thematic maps of large regions of the earth showing predicted artificial V-band sky brightness may be quickly generated with modest computing resources. We have found a fast and accurate method based on previous work to model all-sky quality. We provide limitations to this method. The proposed model meets requirements needed by decision makers and land managers of an easy to interpret and understand metric of sky quality.

1. Introduction and previous work

Sky glow from escaped anthropogenic light degrades visual night sky quality. Sky glow results from reflection and scattering of stray light by molecules and aerosols in the atmosphere. Measurements and models of this phenomenon are useful in evaluating the effect of sky glow on the visual nightscape. This paper develops a method to predict sky glow luminance using Geographic Information System (GIS) analysis applied to readily available remotely sensed upward radiance measures. The result, distance-weighted neighborhood sums of upward radiance around each observation point, have been calibrated with contemporaneous sky brightness measurements of artificial sky glow. The model works best in protected areas distant from major cities and other artificial light sources. It provides an accessible tool to evaluate the amount of sky glow and the quality of the night sky on large landscape scales. The U. S. National Park Service has participated in the development of this tool to advance conservation of scenic resources and the quality of visitor experience.

1.1. Measurements of artificial sky glow

Astronomical observations of background night sky brightness from large observatory telescopes provide one measure of night sky quality. These observations are nearly always of an area near the zenith or the darkest part of the night sky, e.g. [1,2]. Zenith sky brightness has also been measured by citizen science projects and researchers using low cost devices such as the Unihedron SQM and SQM-L. [3–5]. Zenith sky brightness, or zenith luminance (ZL), is important to astronomical observations and is an informative indicator of sky quality in moderate to severely light polluted areas. The U.S. National Park Service (NPS) and natural resource managers characterize the condition of the entire night sky using average sky luminance (or ASL) [7]. This is a more sensitive measure of sky glow because light domes are more intense near the horizon than near the zenith. It is a more relevant measure of sky quality because wildlife and park visitors are more likely to have the horizon in view than the zenith.

* Corresponding author.
E-mail address: sharolyn.anderson@unisa.edu.au (S.J. Anderson).

https://doi.org/10.1016/j.jqsrt.2018.04.028

Accurate measurements of artificial sky glow in areas distant from the sources, may only be obtained when the natural light from the night sky is removed from luminance observations, since the observed sky brightness is the combination of artificial and natural sources. For this reason the NPS developed a method of pixel-by-pixel subtraction of a natural sky model from photometrically calibrated all sky image mosaics [6]. A similar method has been used to improve zenith brightness measures with the SQM-L [7]. Values of 171 µcd m^{-2} and 250 µcd m^{-2} have been proposed as the reference conditions for ZL and ASL, respectively, in the absence of artificial sky glow [8]. These values provide a baseline level for expressing the scale of sky glow. For many audiences, the condition of the night sky is more expressively rendered in terms of a unitless ratio to natural conditions. The ratio indicators utilized in this paper are termed all-sky average light pollution ratio (ALR) and zenith light pollution ratio (ZLR). Numeric indicators of artificial sky brightness were discussed in detail by Duriscoe [8], including their derivation from all sky photometric measurements and application to night sky quality assessments.

To summarize the important sky brightness measures used in this paper, for the hemisphere of sky with azimuth angle φ, zenith angle z, and punctual luminance $B_{\varphi,z}$ in µcd m^{-2}: zenith luminance:

$$ZL = B_{\varphi,0} \tag{1}$$

anthropogenic zenith luminance:

$$ZL_a = ZL - ZL_n \tag{2}$$

where ZL_n= natural sky background brightness at zenith, reference condition set to 171 µcd m^{-2} zenith light pollution ratio:

$$ZLR = ZL_a/171 \tag{3}$$

average sky luminance:

$$ASL = \frac{1}{2\pi}\int_0^{\pi/2}\int_0^{2\pi} B_{\varphi,z}\sin(z)d\varphi\, dz \tag{4}$$

anthropogenic average sky luminance:

$$ASL_a = \frac{1}{2\pi}\int_0^{\pi/2}\int_0^{2\pi} (B - B_n)_{\varphi,z}\sin(z)d\varphi\, dz \tag{5}$$

where B_n = natural sky background brightness at ϕ, z

With the reference condition for the all-sky average set to 250 µcd m^{-2}, all-sky light pollution ratio:

$$ALR = ASL_a/250 \tag{6}$$

It should be noted that the authors know of no observations of night sky brightness that are reported in the ALR metric other than those measured by the NPS camera system. The highly specialized nature of the equipment and its deployment, natural sky model construction, and pixel-by-pixel subtraction technique over the hemisphere severely limit its use. However, these methods are required to tease out the artificial component of sky glow at sites in protected areas remote from the sources, where ALR values below 0.5 are typically observed and create a significant impact [9].

This work is concerned with artificial sky luminance. Illuminance of the landscape will result from this form of light pollution. ASL and ALR are directly related to scalar illuminance, and the products resulting from this work may be interpreted as such. However, horizontal and vertical illuminance from sky glow are not considered.

1.2. Models of artificial night sky brightness

1.2.1. Empirical models

A simplified model of the propagation and scattering of light in the atmosphere was developed by Treanor [10], expanded by Berry [11], and translated into a computer model by Pike [12] in the 1970 s. These models utilized human population as a surrogate for the amount of escaped outdoor light produced by a city. They also included the distance from the observer to the city and a measure of the aerosol content of the air as input parameters. In the late 1970′s, Walker [13] developed a brightness/distance relationship from a source of fixed escaped light from observations of sky brightness at progressively greater distances from the same city. A simple function where the distance is raised to power −2.5 was found to fit the data, the relationship is known as "Walker's Law." This relationship was expanded by Albers and Duriscoe [14] who derived a constant to convert from population to predicted artificial sky brightness for cities. Netzel and Netzel [15] used high resolution daytime satellite imagery classified as "percent of built up area" as a surrogate for escaped artificial light and Berry's empirical model to produce an estimate of sky brightness at zenith over the country of Poland at 100 m resolution with modest computer resources using GIS tools. The model was calibrated with observational sky brightness data from 65 sites. These empirical models paved the way to constructing landscape scale models of the sky brightness at zenith.

1.2.2. Physical models

A complex physical model of atmospheric scattering of light from ground based sources was described by Garstang [16–18]. The model predicts the punctual sky brightness as seen by an observer on earth at any given point in the sky from any number of sources. Garstang's radiative transfer model was adapted to produce the first World Atlas of Artificial Night Sky Brightness in 2001 by Cinzano et al. [19]. Covering most of the land area of earth and using upward radiance data derived from DMSP-OLS satellite imagery as input [20], the atlas is the pioneering landscape-scale assessment of night sky quality based upon a physical model. The New World Atlas of Artificial Night Sky Brightness [7] utilized VIIRS Day/Night band upward radiance data [21] from 2014. The atlas used an enhanced version of the Garstang model [22] was calibrated to thousands of ground based observations over a several year period. Both atlases expressed artificial sky brightness as a ratio to a natural background condition set at 251 µcd/m^2 and 174 µcd/m^2 in the "first" and "new" editions, respectively. Both required substantial computational resources and the assumption of a constant concentration of aerosols over the entire earth.

Physical models have been used to refine the Walker's Law negative exponential zenith brightness/distance relationship. Garstang predicts a variable exponent with distance, ranging from −1.9 to −4.5 at distances of 3 to 100 km, respectively, when earth curvature was considered [17]. Cinzano and Falchi proposed a "general Walker's Law" where B_0 is the night sky radiance near the source and d is the distance in km from the observer to the source:

$$B = B_0 d^{-\alpha} \tag{7}$$

and predicted the value of the exponent α with distance (in km) as an algebraic expression, yielding values between 2.3 and 3.0 for the same distance range as above when the atmospheric clarity k was set to 1.0 [22].

$$\alpha = 2.3\left(1 + \frac{d}{1000}\right) \tag{8}$$

Artificial sky brightness over the hemisphere has also been addressed in modeling efforts, despite the additional computational resources required [22,23]. Luginbuhl, et al. [24] implemented the Garstang model to predict sky brightness at a distance from a moderately large city using an accurate ground based outdoor lighting inventory to define the characteristics of the sources. Duriscoe et al. [23] utilized upward radiance satellite data from the VIIRS Day/Night band to identify artificial lighting location and

amount in a similar study. Five cities for which ground based sky brightness data were compared; the study demonstrated that modeled sky brightness over the entire sky closely matched the observations when the remotely sensed upward radiance data were properly calibrated to the amount of luminous flux employed on the ground.

1.3. A simplified model for landscape scale assessment and monitoring

For rapid assessments over a wide geographic area, the upward radiance monthly cloud-free composites from the VIIRS Day/Night band sensor provide a readily available calibrated source of information on escaped artificial light at night [25]. Data for the entire earth from 2013 to present have been calibrated and prepared for public dissemination, available at https://www.ngdc.noaa.gov/eog/viirs/download_dnb_composites.html. A region of interest may be selected and clipped out, and the grid of upward radiance data may be processed to produce a simplified model of all-sky luminance using an application of the brightness/distance relationship described by previous researchers. By defining a radius of influence for a given observing location, weighting each grid cell's importance to the observer's location according to a brightness/distance function, and integrating weighed measures within that radius, an estimate of the amount of average anthropogenic sky glow visible over the hemisphere may be derived.

For a given upward radiance r_i above each location represented by a raster cell, with the center of the cell's distance from the observer d_i, with n cells within a defined radius of influence, and where the exponent α is dependent upon the distance d, a relationship to the ALR is defined:

$$ALR = c\sum_{i=1}^{n} r_i d_i^{-\alpha} \quad (9)$$

where c is a constant which calibrates the weighted sums of upward radiance to the ground-based observations using the ALR metric.

This method involves certain assumptions (described in Section 2.3) and is a semi-empirical approach. The computational requirements to calculate Eq. (9) iteratively over millions of grid cells in a GIS environment are modest; we sought a method, which would quickly produce a model of high confidence to be applied over a wide geographic area repeatedly over time, corresponding to monthly releases or yearly averages of the remotely sensed radiance data.

2. Methods

2.1. Analytical approach

This study utilizes a brightness/distance relation verified by a Garstang model experiment and ground based observations, contemporaneous observations of upward radiance (from an orbiting satellite) and observed artificial sky brightness (from the ground), GIS processing algorithms automated from available tools, and accurate calibration to observed all-sky data representing the artificial sky glow only (ALR). The purpose and design of the research are shown as a flowchart in Fig. 1 and summarized below along with reference to the section numbers where each item is described. The work is divided into three separate tasks (A, B, and C) each with sequential steps leading to the product:

A. Define the brightness/distance relationship for the ALR metric
   1. Utilize a modification of Cinzano and Falchi's "general Walker's law" as the functional form to be fitted (§1.2.2).
   2. Conduct a Garstang modeling experiment over the entire sky on a single city (Las Vegas) to predict the brightness/distance relationship for ALR (§2.4, §3.1)
   3. Utilizing existing NPS data and directed field data collection at measurement sites representing a variety of distances from the Las Vegas city center to verify the modeled results (§3.1).
   4. Examine the fit of the Garstang model results to the observations and adjust the function if necessary (§3.1).

B. Test the validity of the ALR/distance relationship with directed field observations in the southwestern United States
   1. Identify measurement sites outside of developed areas (§2.2.1).
   2. Collect data only on nights of low aerosol conditions as near local midnight as possible (§2.2.1)
   3. Extract summaries of VIIRS radiance data as a function of distance using the function developed in task A for each of the measurement sites, with monthly composites contemporaneous with field data collection (§2.2.2, §2.5).
   4. Examine the fit of observed ALR to the weighted sums of upward radiance for each site and compute the calibration constant using linear regression (§3.2).

C. Produce tools to predict sky luminance metrics at points or project them across landscapes (§2.5, §3.2, §4.2, §4.4).

2.2. Data sources

2.2.1. Sky brightness observations

Observational data from 24 locations throughout the western United States were selected for model verification. Field data was collected with the U.S. National Park Service all-sky mosaicking CCD camera system [26]. Two directed data collection efforts were conducted, one in January-March 2015 in the Los Angeles, California area and one in May-June 2016 in the Las Vegas, Nevada area. Sites were selected involving a variety of distances from the metropolitan areas. Data were obtained only on nights of high atmospheric transparency, and locations completely surrounded by development were excluded, following the recommendation of Cinzano and Falchi [22]. In addition, a selection of sites from the National Park Service database quite remote from large cities was included from locations in Arizona, Colorado, and Texas. The time period of the observations encompassed the range September 2014 to February 2017. Table 1 lists each site, including the name, date, geographic coordinates, observed average artificial sky luminance (ASL), and derived ALR and ZLR.

2.2.2. Upward radiance observations

VIIRS Day/Night band monthly cloud-free composites generated by Earth Observation Group, NOAA Centers for Environmental Information were used for upward radiance measurements. These composites are average Day/Night band radiances for observations deemed cloud-free and collected under new moon conditions. For this study the stray-light corrected composites were used, which gives complete monthly coverage for the conterminous United States. In order to reduce possible differences between the remotely sensed upward radiance and ground based observations of sky glow, the two collections should be as close to simultaneous as possible. We used the monthly cloud free composite corresponding to the CCD camera measurements of sky brightness observations in this work. Eleven different monthly cloud-free composites were required to pair with the CCD observations.

Natural sources of upward luminance, primarily atmospheric airglow, are variable and produce background "noise". This noise is captured in the VIIRS data and can vary between days and months (Fig. 2). To adjust for this, the background value less than 0.5 $nWcm^{-2}\ sr^{-1}$was set to zero. With a reported instrument noise of

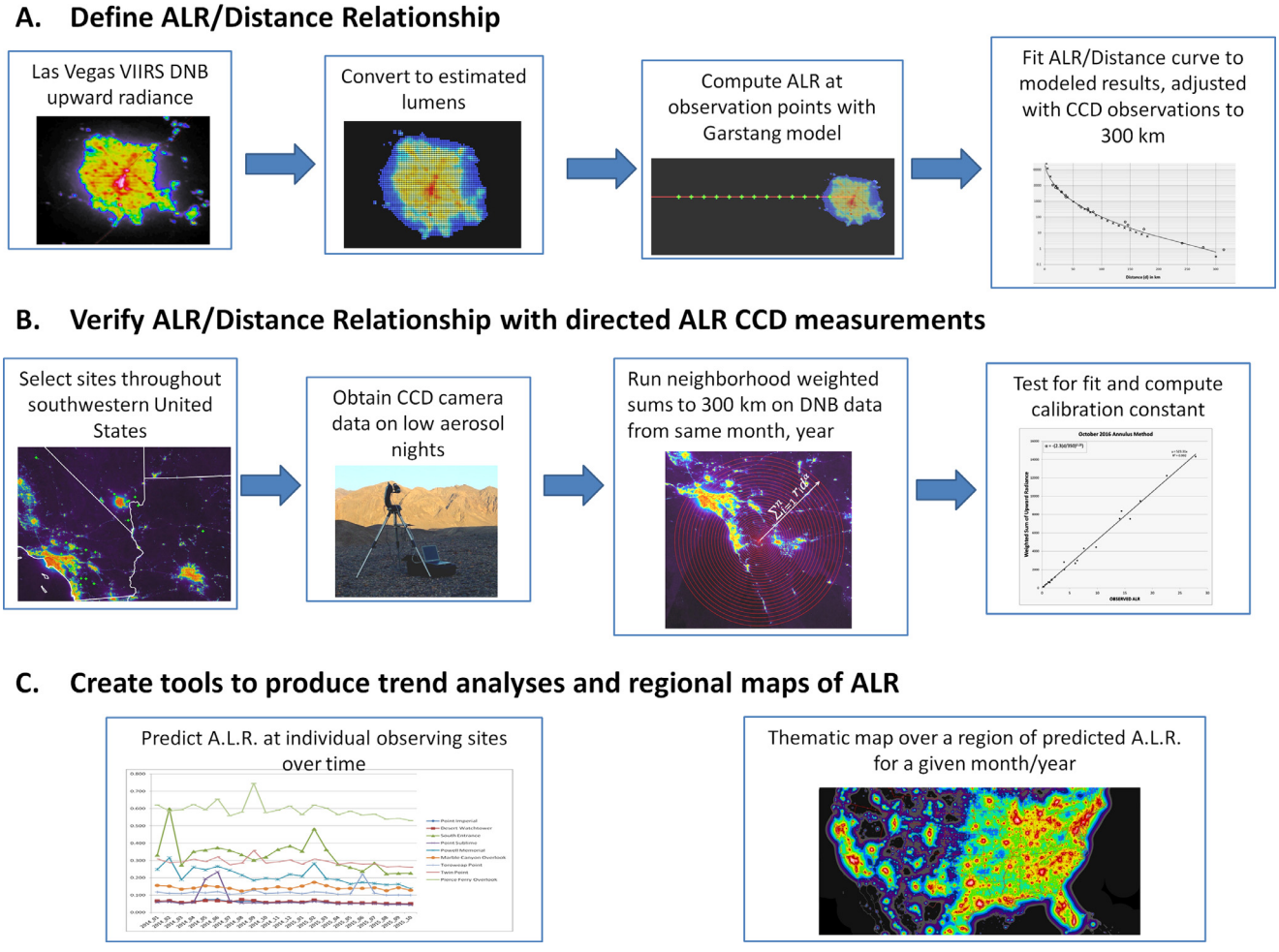

Fig. 1. Flowchart demonstrating the three main tasks included in this paper and the steps involved to creating the products.

Table 1
Sky brightness measurement sites, locations, average artificial all-sky luminance (ASL), all-sky light pollution ratio (ALR), and zenith light pollution ratio (ZLR), as measured by the V band NPS CCD camera. Sorted on ALR darkest to brightest sites.

Site	Date (UT)	Longitude	Latitude	ASL (μcd m^{-2})	ALR	ZLR
San Joaquin Ridge, California	17-Jul-2015	−119.0639	37.6800	38	0.15	<0.10
Ashurst Lake, Arizona	09-Jul-2016	−111.4309	35.0271	67	0.27	<0.10
Mesa Verde N P, Colorado	25-Sep-2014	−108.3674	37.2363	77	0.31	<0.10
Enchanted Rock S P, Texas	18-Aug-2015	−98.8240	30.5028	137	0.55	0.17
Rocky Mountain N P, Colorado	13-Aug-2016	−105.7240	40.4143	195	0.78	0.14
Cottonwood Cove Rd, Lake Mead N R A, Nevada	29-May-2016	−114.7902	35.4713	278	1.11	0.21
Marine Corps Training Center, California	24-Feb-2017	−116.2557	34.3103	324	1.30	0.25
Anza Borrego Desert S P, California	22-Mar-2015	−116.2892	33.1636	331	1.33	0.34
Temple Bar Airstrip, Lake Mead N R A, Arizona	30-May-2016	−114.3353	36.0043	348	1.39	0.22
Echo Bay Airstrip, Lake Mead N R A, Nevada	01-Jun-2016	−114.4693	36.3201	424	1.69	0.33
Johnson Valley, California	18-Feb-2015	−116.6659	34.3859	442	1.77	0.64
Puerta La Cruz Rd, California	18-Jan-2015	−116.6451	33.3402	577	2.31	0.40
Lucerne Valley, California	18-Feb-2015	−117.0683	34.4444	991	3.96	1.09
Palomar Observatory, California	14-Feb-2015	−116.8602	33.3487	1,008	4.03	1.08
El Mirage Dry Lake, California	18-Feb-2015	−117.5579	34.6353	1,499	6.00	1.78
Ramona, California	14-Feb-2015	−116.8792	33.1235	1,593	6.37	1.99
Tule Springs N M, Nevada	02-Jun-2016	−115.4154	36.4259	1,891	7.56	2.22
Calville Bay Turnoff, Lake Mead N R A, Nevada	01-Jun-2016	−114.7528	36.1836	2,448	9.79	2.01
Lake Elsinore, California	15-Feb-2015	−117.3632	33.6216	3,518	14.07	5.10
Lakeview, California	16-Feb-2015	−117.1080	33.8285	3,603	14.41	6.03
Government Wash, Lake Mead N R A, Nevada	01-Jun-2016	−114.8338	36.1517	3,990	15.96	4.96
Canyon Lake, California	15-Feb-2015	−117.2692	33.7130	4,452	17.81	7.29
San Gabriel N M, California	13-Feb-2013	−117.7591	34.2180	5,650	22.60	7.72
Mt. Charleston Rd / Hwy 95 Jct., Nevada	02-Jun-2016	−115.3069	36.3277	6,960	27.84	10.35

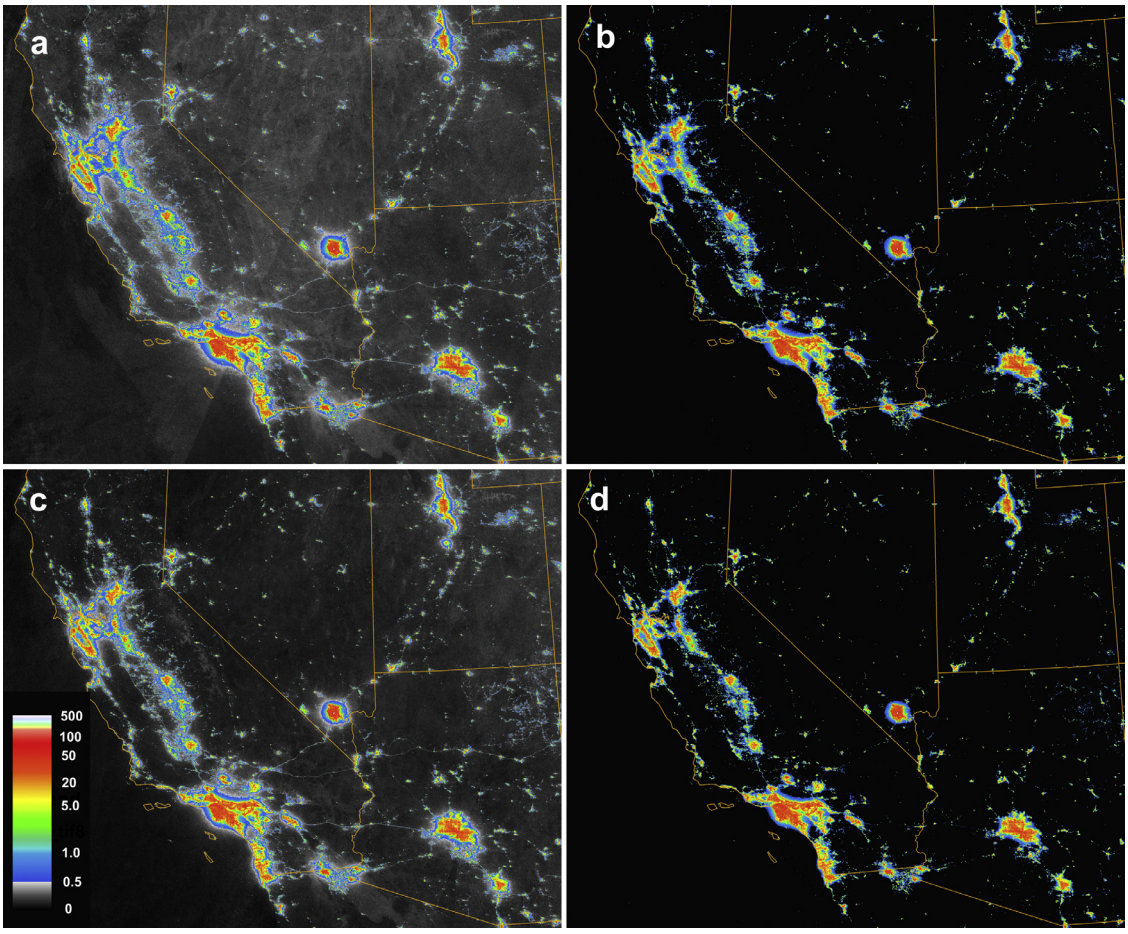

Fig. 2. (a) stretched October 2016 monthly composite; (b) October 2016 monthly composite with background noise removed (pixels < 0.5 set to 0.0); (c) stretched November 2016 monthly composite; and (d) November 2016 monthly composite with background noise removed (pixels < 0.5 set to 0.0). (For interpretation of the references to color in this figure, the reader is referred to the web version of this article.)

0.1 nW cm^{-}2 sr^{-1}, this value is consistent with the concept that a signal to noise ratio of at least 5 is required to verify a source of upward radiance from the ground [27,28].

Fig. 2a and c show that there is less background noise in November than October, but clipping at 0.5 (Fig. b and d) successfully removes it in both cases revealing only the cities and towns. Also, after clipping, the halos around bright cities (blue) are still seen representing the scattering of light by the atmosphere beyond the light sources and the halo west of Los Angeles is larger in October than November indicating more scattering.

The downloaded datasets are in geographic coordinate systems. We re-projected to gnominic (for single observation points) or Albers Equal Area (for creating maps of large regions) so each cell is equally represented when upward radiance values are summed. When working with the distance and area calculations it is more accurate to work in the appropriate projection.

2.3. The neighborhood sum algorithm

An application of the brightness-distance relationship for artificial sky glow described by Eq. (9) is the fundamental basis of the simplified model. Each grid cell in the upward radiance data set within a certain radius of influence around an observing site is assumed to contribute to the ALR additively according to this relationship. A radius of influence around each observation point was selected based upon theory, observations, and practicality. Cinzano and Falchi [22] suggest that distances up to 350 km should be considered. Observations with an all-sky camera from high mountain sites under low aerosol conditions reveal sky glow readily visible from large cities up to 300 km away (see Fig. 3). While relatively bright, the observed light dome of Las Vegas as seen from Great Basin National Park is quite small, and contributes less than 2% of the natural background brightness to the all-sky average. Therefore, a premise is adopted that the exponent α in the brightness/distance relationship is variable with varying distance from the source. Thus, near the source becoming progressively more negative as the distance is increased, and at greater distances, up to 300 km, will be between 2 and 2.5.

2.4. Defining the brightness/distance function with a modeling experiment

An extended light source was constructed for a modeling experiment to determine the brightness/distance relationship for the ALR metric. This task builds upon the work of Duriscoe et al. [23]. VIIRS Day/Night band (DNB) upward radiance data for the Las Vegas Metro area from 2012 was used to determine the position (latitude, longitude) and luminous flux of the source on the native VIIRS DNB pixel grid. A sky glow model developed by Garstang [16,18] and modified by Luginbuhl et al. [24] was used to predict the sky luminance over the hemisphere at distances from the city center between 20 and 300 km. The input luminous flux to this model must be in lumens; the upward radiance values were converted to estimated installed lumens in each grid cell using the conversion 3698 lm W^{-1} sr [23]. Other model parameters, set as described in the above reference, include the angular distribution

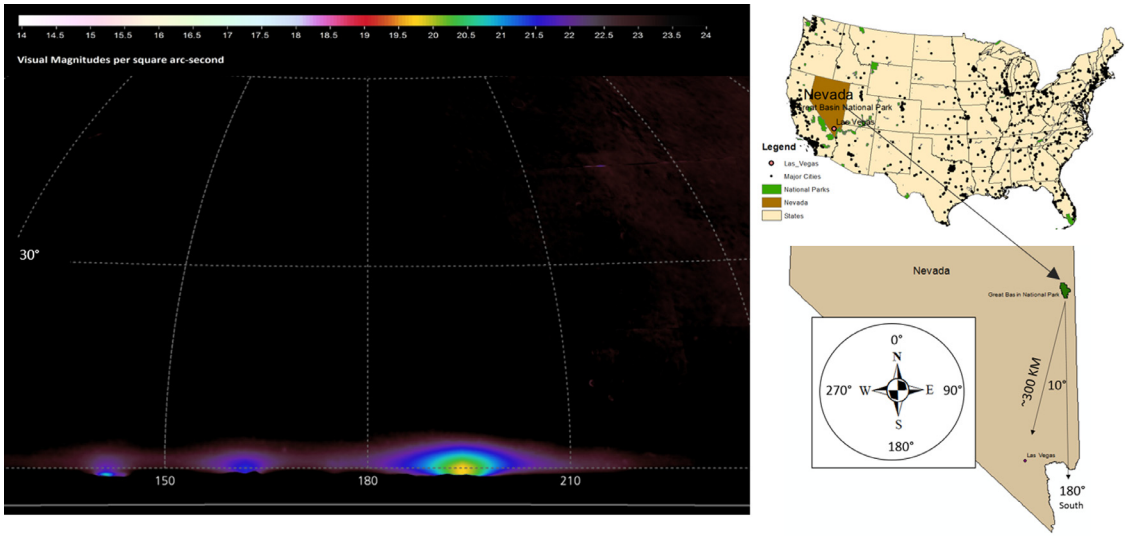

Fig. 3. Portion of the all-sky brightness mosaic showing the light dome of Las Vegas, Nevada, metro area at azimuth 190 as seen from Great Basin National Park, 311 km distant. From this high vantage point a portion of the sky is below the level horizon (dashed gray line), and the appearance of the light dome may be influenced by atmospheric refraction.

of upward emitted light as defined by Garstang [16] with a ground reflection of 0.15 and direct uplight fraction of 0.10, and a blocking profile (blocking parameters $Eb_b = 0.3$ and beta = 0.1) arising from the blocking of light rays by objects in the near-ground environment as described by Luginbuhl et al. [29]. The aerosol content of the atmosphere was set using the Garstang K parameter K = 0.35.This is a key assumption yet based on low atmospheric aerosol conditions which are typical of the western United States. Note this differs significantly from the use of K = 1.0 in the New World Atlas [7].

For sites closer than 20 km the brightness/distance relation was corrupted by the breakdown of the simple observation point – city distance relation due to the extended nature of the city source. Thus for distances of 20 km and less an alternative source consisting of the same luminous flux as the extended model but located at a single (Central) location was used. This point-source model was confirmed to give the same values at distances greater than 20 km as the extended-source model based on the DNB image.

Outputs from the model included predicted anthropogenic sky brightness over the entire sky on a 2° grid, from which ASL and ALR at each distance were computed. In this manner a brightness/distance relationship was derived for ALR and ZLR. A curve described as a function involving only distance *d* in km was fit to the model output.

2.5. GIS neighborhood analysis methods

Two different methods for computing the brightness/distance relationship in a spatial environment were developed. Both use tools available in ESRI™ ArcGIS 10.x software. Both use raster datasets created from DNB cloud-free composites.

Method 1 utilizes the Euclidean Distance method to compute the distance from a defined observing site to each cell in the raster. It is appropriate when a collection of sites of interest and their geographic coordinates are available, providing a very rapid computation on a cell-by-cell basis. The DNB image is first clipped to include the region around the each observing site to at least 300 km in all directions, then projected using the site's coordinates as the center of a gnomonic projection. The distortion introduced is maximum at the 300 km distance, and is less than 0.07% in radial distance. The surface of the earth is thus converted to a flat plane to which Euclidean geometry may be applied without significant error. After the distance to each cell is computed, it is raised to the power predicted by the brightness/distance relationship equation, producing a weighting factor for the radiance value of each cell. Raster multiplication (upward radiance x weighting factor) yields the weighted radiance values, which are then summed over the 300 km radius circle around the observing site.

Method 2 utilizes the Neighborhood Annulus method and simplifies the calculations by assuming all cells within one ring around an observing site are at the same distance from that site. It takes a cloud-free VIIRS image that is clipped and projected into Albers equal area conic projection for the area of interest. It then runs a loop for the specified number of annulus rings away from each pixel for estimated influence. We used 38 rings out to 300 km. The second data input for the model is a table with the weights for each ring calculated using the brightness/distance relationship and the average radius of the ring. The sum of the upward radiance values of the cells within each ring is obtained and multiplied by the weighting factor from the table. The raster datasets from all 38 rings are then summed to produce a map of weighted sums over a region (Fig. 4).

The two methods model the ALR either for specific points (Euclidean Distance) or for an area of interest (Neighborhood Annulus). The two methods were optimized for the desired results, a table or a map layer.

Note that in the Garstang model experiment, the upward radiance values in the DNB grid were first converted to lumens on the ground using a calibration constant from previous work. The GIS neighborhood analysis method does not, and the calibration constant must be converted to ALR after the fact. A least squares linear regression forced through the origin was used to correlate observations (considered the independent variable) of ALR with the sum of weighted upward radiance values from the model algorithm (the dependent variable) at the observation locations. After dividing the model output by the calibration constant (the slope of the regression line), predicted values in ALR are obtained.

There were 24 field sites used for the least squared linear regression. Although that is a sufficient number of samples, it was decided that a bootstrap technique was preformed to better understand the model. The technique is a general approach to statistical inference using the data at hand and resampling data to further examine the selected model. We found a confidence interval of ad-

Table 2
Modeled average artificial sky brightness versus distance from Las Vegas, Nevada. Natural background values of 250 and 171 μcd m^{-2} were used to calculate the ratios ALR and ZLR for all-sky and zenith, respectively. The ratio of the indicators ALR / ZLR is shown in the last column.

Distance from Las Vegas (km)	ASL (μcd m^{-2})	ALR	Zenith Luminance (μcd m^{-2})	ZLR	ALR/ZLR
3	2.57 E+06	1,027.46	9.42 E+04	550.68	1.87
5	1.22 E+05	488.14	3.88 E+04	226.63	2.15
10	3.74 E+04	149.52	9.62 E+03	56.23	2.66
20	9.74 E+03	38.97	2.25 E+03	13.16	2.96
30	3.87 E+03	15.36	8.56 E+02	5.01	3.07
40	1.81 E+03	7.23	4.01 E+02	2.35	3.08
50	9.61 E+02	3.84	2.07 E+02	1.21	3.07
60	5.48 E+02	2.19	1.17 E+02	0.68	3.02
70	3.24 E+02	1.30	7.03 E+01	0.41	3.15
80	2.00 E+02	0.80	4.46 E+01	0.26	3.07
90	1.29 E+02	0.52	2.95 E+01	0.17	2.99
100	8.56 E+01	0.34	2.01 E+01	0.12	2.91
110	5.83 E+01	0.23	1.41 E+01	0.08	2.82
120	4.07 E+01	0.16	1.01 E+01	0.06	2.75
130	2.88 E+01	0.12	7.38 E+00	0.04	2.67
140	2.07 E+01	0.08	5.47 E+00	0.03	2.59
150	1.51 E+01	0.06	4.11 E+00	0.02	2.51
160	1.10 E+01	0.04	3.13 E+00	0.02	2.41
170	8.18 E+00	0.03	2.41 E+00	0.01	2.33
180	6.08 E+00	0.02	1.87 E+00	0.01	2.23
300	3.25 E+00	0.00	1.34 E-01	0.00	1.66

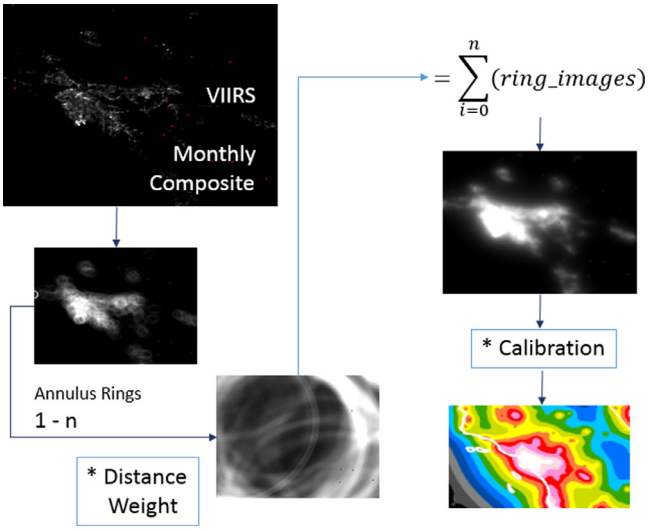

Fig. 4. The flowchart for the python script that creates the dataset (a TIFF image) of ALR values for the area of interest. The weights per annulus ring used the median distance for radius and Eq. 3 for exponent.

justed R squares from 0.9788 to 0.9982 verifying the validity of the linear model.

3. Results

3.1. Prediction of brightness/distance relationship

The results of the Garstang model calculations described in Section 2.4 are shown in Table 2. The table uses the values of 171 μcd m^{-2} and 250 μcd m^{-2} as the reference conditions for zenith and average sky luminance in the absence of artificial sky glow.

From the above model products, the Walker's Law exponent was derived using the formula:

$$\alpha = -LOG_d(ALR/i) \quad (10)$$

The constant i is somewhat arbitrarily set, depending upon the desired value of α at a given distance d. As a starting point, we set the constant to produce $\alpha = 2.6$ at $d = 300$ km. The suite of x, y points (d, ALR) derived in this manner was fit to a curve with an algebraic expression which is a modification of Eq. (8), producing a nearly exact fit to the modeled results. However, when the predictions were compared to ground-based observations out to 311 km from Las Vegas city center, the sites more distant to the cities were consistently under-predicted by the model. We therefore iteratively explored further modifications to Eq. (8) to achieve the best fit, ultimately arriving at the following:

$$\alpha = 2.3\left((d/350)^{0.28}\right) \quad (11)$$

The observed and predicted ALR for a wide range of distances from Las Vegas city center are shown in Fig. 5, including the curve defined by Eq. (11). The modeled results were scaled to match the observed at $d = 40$ km. The range of the exponent -α determined by Eq. (11) is from −0.45 at 1 km to −2.20 at 300 km. ALR observations at the more distant locations were derived from summing luminance values on the all-sky CCD mosaic for the Las Vegas light dome only, eliminating contamination from other cities (see Fig. 3).

It appears from Fig. 5 that the Garstang modeling experiment significantly under-predicts the ALR at distances greater than 100 km from the city center. This may be because of any or all of the following factors; the observations were taken under lower aerosol conditions than those set for the model, the direct escaped light from the city at angles close to the horizontal may be greater than the parameters set for the model describe, or the model may have inherent flaws in predicting sky glow near the horizon. The brightness/distance function selected attempts to match the observations at distance while maintaining the general form of the function for α described by Eq. (8).

3.2. GIS model construction and calibration

The expression for the Walker's law exponent produces a weighting of upward radiance from any cell in the DNB raster as a function only the distance from the observer to that cell. Using the "Euclidean distance method", weighted sums were computed for each of the 24 observing sites from the contemporaneous monthly cloud-free composites. A linear regression of observed vs. predicted reveals an excellent correlation (Fig. 6). The slope of the line, 562.72, is the calibration constant C in Eq. (9) which converts the weighted sum to ALR.

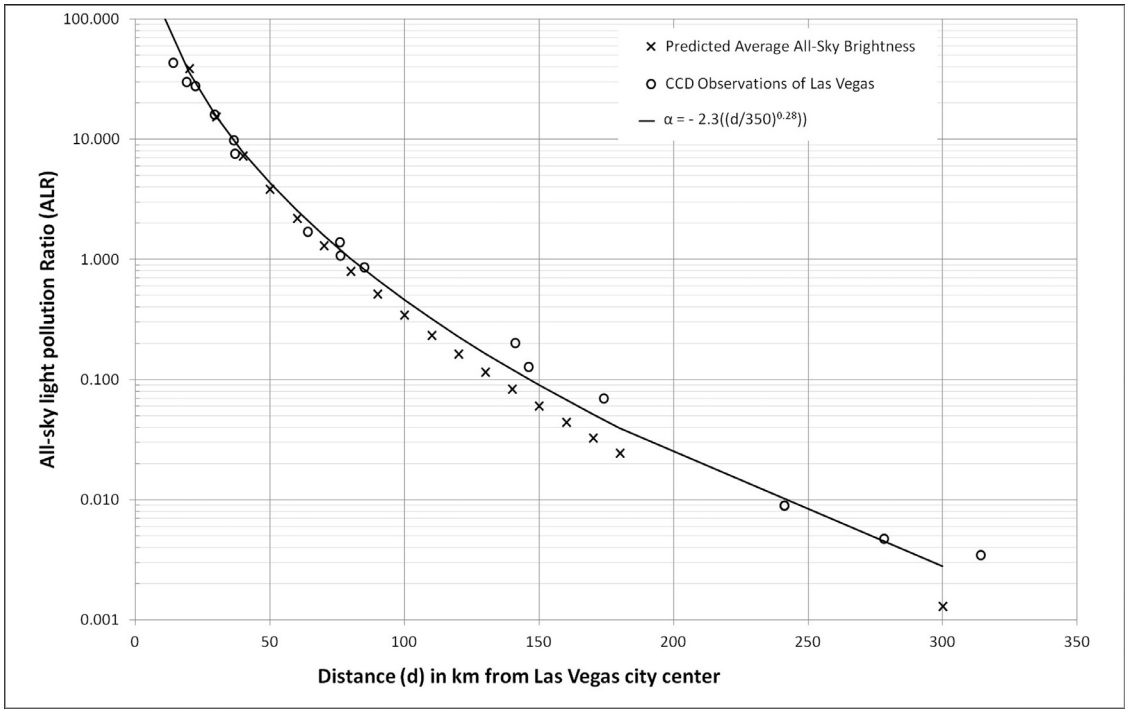

Fig. 5. Plot of modeled and observed all sky light pollution ratio at distance from the Las Vegas, Nevada, metropolitan area. Note the logarithmic scale on the vertical axis.

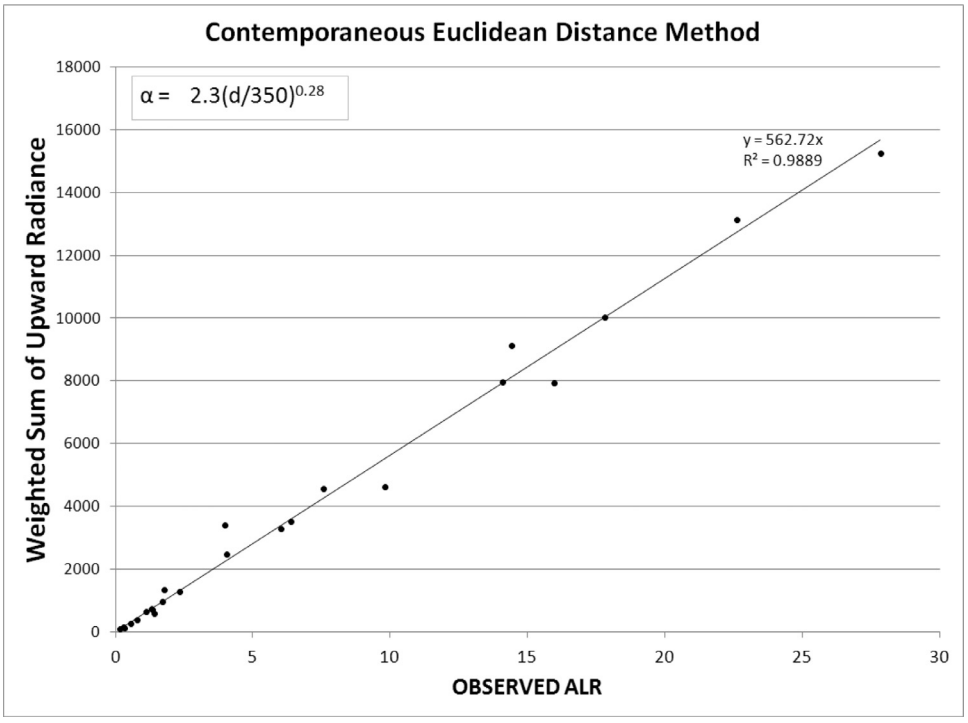

Fig. 6. Correlation of the a linear regression of observed ALR vs. predicted weight sums of VIIRS radiance.

Using the "Neighborhood annulus method" described in Section 2.5, a thematic map of predicted ALR for the conterminous United States was produced using multi-threading on an 8 core PC in approximately one hour. A weighted sum raster over the region is produced at a resolution of 450 m, divided by the calibration constant, and 300 km from each edge is cropped out to eliminate the buffer areas. A result using the October 2016 monthly composite is shown in Fig. 8(B) using a color map showing the ratio to natural. Fig. 8(A) shows the same region with predicted zenith sky brightness from the New World Atlas of Artificial Sky Brightness [7].

Comparing the ALR model to the New World Atlas (Fig. 7B and 7A) the first impression is that the light pollution impacts are more severe. This is to be expected when the entire sky is considered,

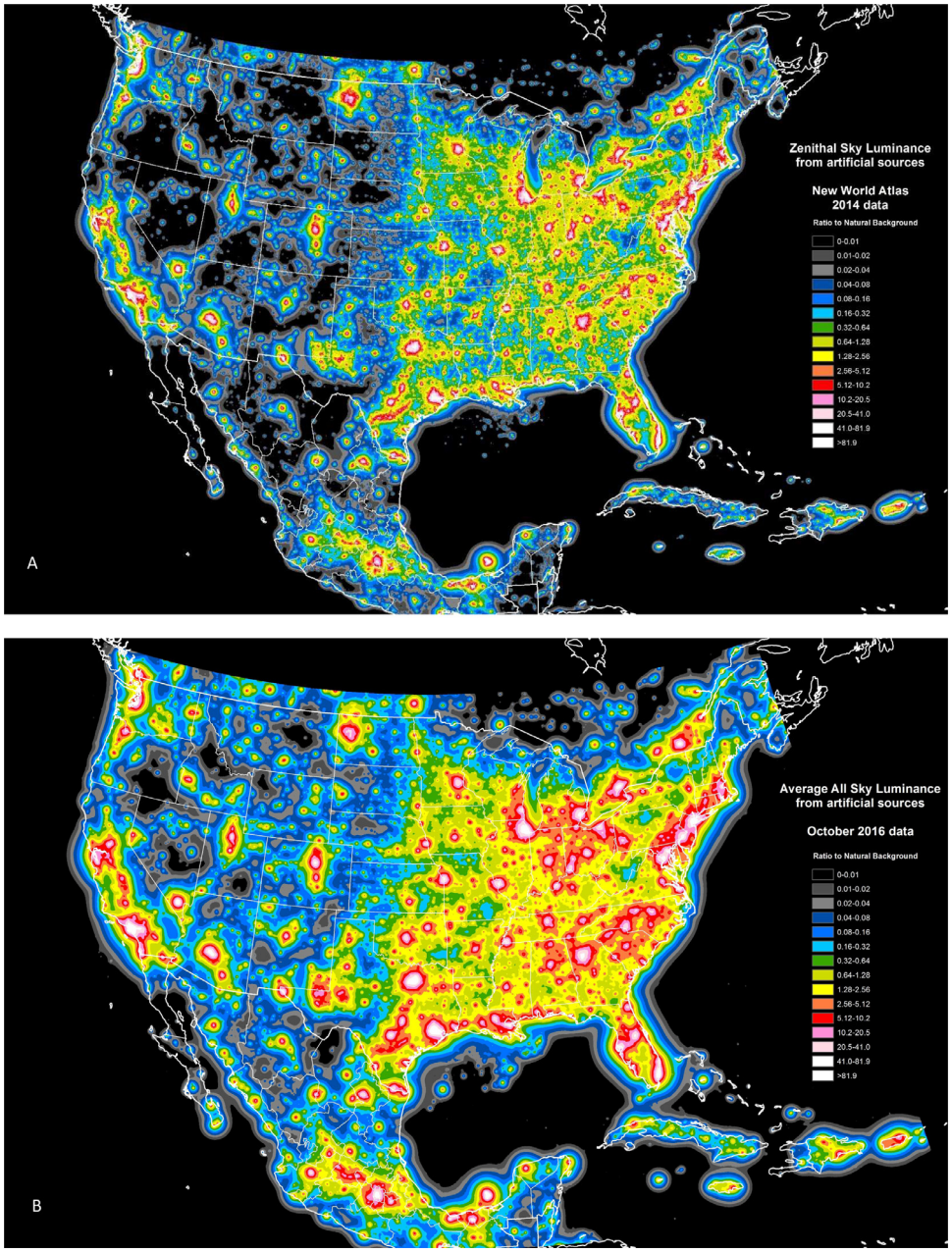

Fig. 7. Comparison of the (A) predicted Zenith Sky Brightness reproduced from the New World Atlas of Artificial Sky Brightness and the (B) predicted All-Sky Luminance Ratio from the simplified model presented in this work over the conterminous United States.

since artificial sky glow typically becomes progressively brighter from zenith to horizon. If one is looking for locations where only the zenith is relatively unaffected, the New World Atlas will be a better source. However, it is possible to derive a ZLR/distance relationship and utilize the neighborhood analysis to produce a ZLR map, if desired. The primary difficulty is differentiating the artificial component of zenith brightness from the natural background in field observations using broadband photometry under low artificial sky glow conditions. The natural airglow is highly variable and difficult to model, leading to significant potential errors when it is at its brightest [6]. A practical measurement lower limit is perhaps 10% above natural. In these circumstances, a physical model such as the New World Atlas would provide a more accurate estimate. Any other indicator of interest, with a higher "signal to background noise," such as horizontal illuminance or an average luminance within a specified area of the sky around the zenith, may similarly be investigated. For protected areas, such as national parks, the entire hemisphere of sky, represented by ALR, is the most unbiased metric.

4. Discussion

4.1. Comparing light pollution ratios

Hollan [30] emphasized the use of ratio of artificial to natural conditions as a means of describing environmental impacts. The "world atlases" of artificial night sky brightness established the zenith artificial sky brightness ratio to natural (ZLR) as a popular indicator. The modeling experiment described in Section 2.4 and summarized in Section 3 predicts that the ALR is always higher

Table 3
Classes of visual sky quality, combined from U.S. National Park Service and New World Atlas of Artificial Sky Brightness, showing ranges for ALR and ZLR described in the text. NELM is "naked eye limiting magnitude," or the faintest detectable star for visual observers of the night sky.

Sky Quality Class	ALR	ZLR	NELM	Bortle Class	V band zenith sky brightness (mags arcsec^{-2})	New World Atlas Visual Impact Class
Good	0–0.33	0–0.1	6.8–7.6	1–3	>21.90	Black, blue
Moderate (threatened)	0.33–2.0	0.1–0.7	6.3–6.7	4	21.90–21.45	Green
Poor (for sensitive protected areas)	2.0–10.0	0.7–4.0	6.2–5.7	5	21.45–20.50	Yellow
Milky Way invisible	> 10.0	>4.0	<5.7	6–9	<20.50	Red, white

than the ZLR, by a factor of 1.58–3.27. Sky brightness measurements have shown that ALR/ZLR is highest in the darkest locations, and that the range is 2.0–6.0 (see Table 1 and [8]). Thus the ALR is a more sensitive indicator in darker locations, and has greater applicability to an assessment of visual quality in protected areas.

4.2. Interpreting the model output in terms of visual night sky quality

For protected areas such as in many US national parks and wilderness areas, a high standard of “naturalness” is expected, especially in terms of visual quality or “scenery.” Moore et al. [31] proposed standards for visual night sky quality for “higher sensitivity parks” in terms of the ALR indicator, where < 0.33 is good condition, 0.33–2.0 is moderate condition, and > 2.0 is poor condition. They summarized these classes in terms of other common metrics of night sky quality and a narrative in a table, parts of which are reproduced in Table 3. We add an additional class, following the assessment of visual sky quality in the New World Atlas of Artificial Sky Brightness (Fig. 10 in [7]). A separation is made when the Milky Way becomes invisible at ZLR 4.0, corresponding approximately to ALR 10.0.

4.3. Limitations

A simplified model necessarily carries with it a variety of assumptions and limitations which may affect the accuracy of the predictions. Deviations from assumed conditions of the spectral power distribution of sources, ground reflectance, and aerosol content of the atmosphere are a few potential sources of error in the model predictions. These are examined in the following sections.

4.3.1. Spectral issues

An implicit assumption of this model is that the spectral power distribution (SPD) of all communities, that is, the mix of lamp sources used within each community, is the same or similar. If this assumption is violated, that is some particular community or light source has a significantly different mix of lamp types and thus SPD than the average, the measured and predicted sky brightness may significantly deviate from the calibration. The spectral response of the VIIRS DNB and National Park Service V band camera (NPS_V) are shown in Fig. 8. The V-band response extends approximately 10 nm bluer than the DNB, but an even more dramatic difference in the red and near infrared means that the DNB sensor will be much more sensitive to red sources (e.g. incandescent sources, including flames). Though the fact that CCD observations from two different large metropolitan areas, Los Angeles and Las Vegas, both fell on the same regression line when compared with the DNB weighted sums provides some reassurance that averages may not range widely for large communities, the effect for smaller cities or isolated sources may or may not be negligible.

The propagation over long distances of light giving rise to artificial sky glow is also wavelength dependent. Just as the setting sun looks redder than when overhead, distant light domes will be progressively reddened. This implies that cities employing outdoor lighting with a bluer SPD will measure dimmer in V band at distance than those using redder sources [32]. This limitation can also been seen when street lights in a city changed from yellow/orange (sodium vapor) to white (LED), the radiance observed by the VIIRS DNB decreases. This is due to the sensor’s lack of sensitivity to light in the bluer range of 400 to 500 nm. As high-pressure sodium (HPS) area lighting is replaced with a technology with a different SPD, namely white LED, this effect may lead to an under prediction of ALR for sites remote from the sources. It is important to understand that visual sky brightness to the dark-adapted eye, however, remains bright even for bluer sources [32]. For a more in-depth discussion of spectral limitation see appendix A.

4.3.2. Inherent variation in DNB monthly composites

An objective of the model is to track changes in sky quality over time resulting from changes in artificial upward radiance. However, it is possible that month to month changes in the DNB data for a particular grid cell or source do not correspond to actual on the ground changes in outdoor lighting amounts. There are a number of known and potential reasons for this, the most easily recognized one is a change in surface reflectance from a known cause. Snow cover during winter months can dramatically change the amount of upward radiance from outdoor lighting, and can usually be identified and avoided. Surface reflectance changes from other causes are possible and may not be identifiable, including vegetative cover (including deciduous foliage) and changes in developments such as buildings and roads [33]. Anomalies may be introduced by atmospheric scattering and near-field scattering in the instrument; it was shown that for point sources such as ships at sea the signal on the DNB image is described by a point spread function encompassing as many as 24 pixels [34]. This implies that aggregating the data before analysis may produce more consistent results. The same study followed "static" sources including bridge lights and a moderately large city and found significant variability over time, which they attributed to variations in lunar illumination, geo-location errors, and errors in stray light correction of the instrument. Some of these factors have been accounted for and removed to produce the "VIIRS Nighttime Lights" or VNL DNB grid [25]. To date a yearly average for 2015 has been produced. In future, the VNL grids may provide a more accurate source for tracking changes in artificial lighting and its effects over time, although only on a yearly basis.

Possibly the most important and intractable issue is the influence of atmospheric scattering and absorption. Several studies have investigated this, some with the objective of quantifying the aerosol concentration or optical depth over cities [35–37]. Without a correction for the variation in transmissivity of the atmosphere from night to night or monthly average to monthly average, inherent variations in upward radiance from stable light sources will be observed.

Upward radiance from atmospheric scattering is also observed by the DNB detector. This is particularly apparent when a large city or other bright source is adjacent to a water body or other area with no artificial sources. To our model, the scattered light is

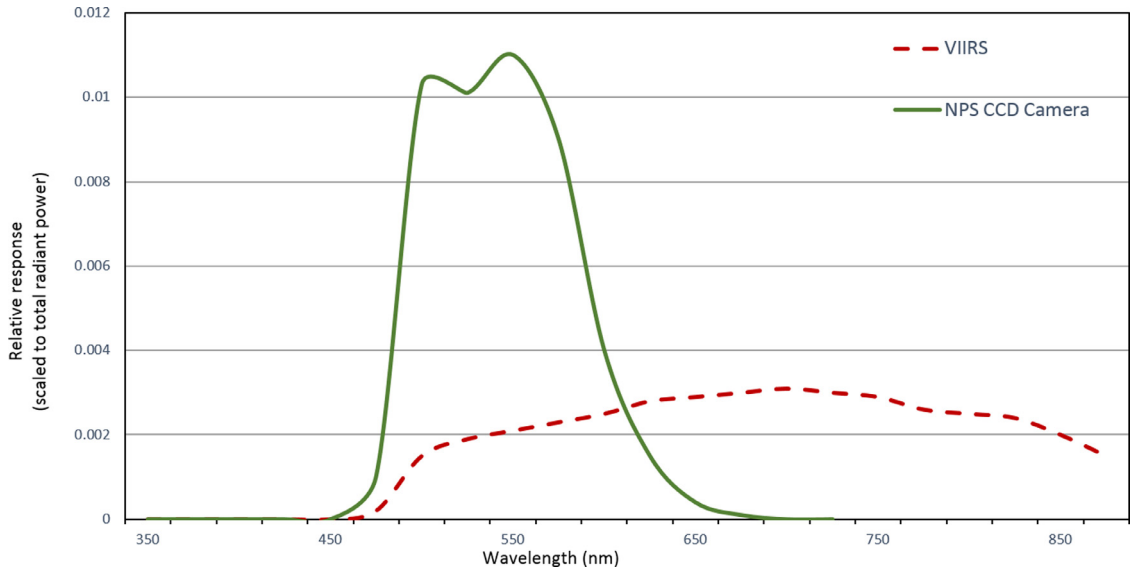

Fig. 8. Comparison of the spectral sensitivity of each of the two detectors used for ground based and remote observations of upward radiance and its effect upon visual sky glow.

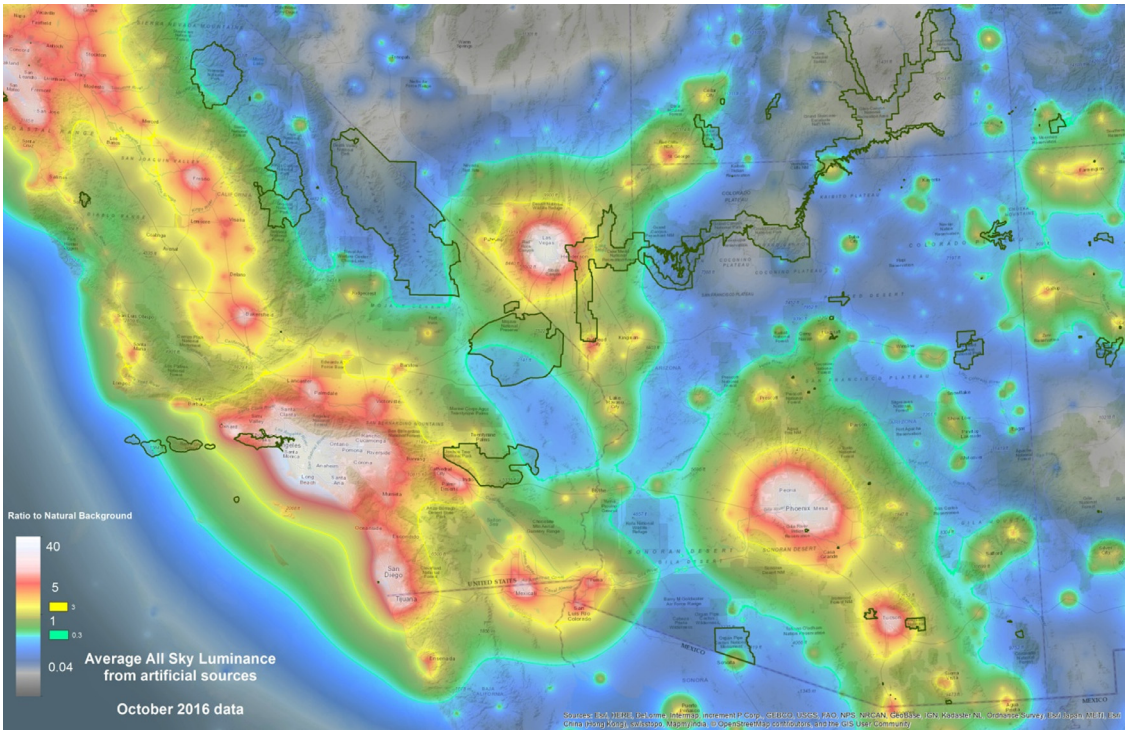

Fig. 9. High resolution map of the southwest U.S., showing predicted artificial sky brightness (ALR) and protected areas administered by the U.S. National Park Service. The bright turquoise and yellow bands identify two threshold values of ALR, 0.3 and 3.0, corresponding to good and poor night sky quality (Table 3). (For interpretation of the references to color in this figure legend, the reader is referred to the web version of this article.)

interpreted as a source on the ground, and can lead to an overestimation of sky glow at sites near the city/water boundary.

4.3.3. Model parameters are fixed, the real world is variable

The uplight function of the sources, the aerosol content of the atmosphere, and terrain and local blocking are all highly variable from day to day or region to region. This model predicts a "worst case" in some ways because of the conditions of the field data collection. Many of the calibration sites were deliberately picked to be free of local blocking, on mountaintops, and in desert environments with sparse vegetation. They were also selected from nights with low aerosol content in the atmosphere. Under higher aerosol concentrations brighter sky conditions near the source and less bright distant from the source would be expected. If outdoor lighting sources are replaced with fixtures that are equipped with better shielding from direct uplight, artificial sky glow will decrease. The use of a simple formula for the brightness distance relationship allows a straightforward method for re-calibrating the model to fit a variety of conditions, if necessary, by varying the numeric constants in Eq. (9) as conditions change.

4.4. Applications

Early studies in light pollution were directed by the astrophysical research community and mainly focused efforts on measurements at the zenith. These were vital studies as the population and outdoor lighting increased. The 1970 s research agenda was not focused on the effects of light pollution in the nocturnal environment more broadly nor the ecosystems that are affected [25]. As the effects of light pollution (artificial light at night) on human health, as well as, its consequences on the flora and fauna are being identified, a broader understanding of the entire night sky is needed. The applications of this modeling effort are essential for easy interpretation of night skies, landscape assessment, management decisions and tracking changes in artificial lighting at night.

The interaction of the artificial light at night and its surround environment are multifaceted and multidimensional. The physics of light, spectral properties, and propagation through the atmosphere are complex and yet not essential for decision makers or application use. To address these needs we present the Simplified All-sky Light pollution Ratio (SALR) model, which is based on physical properties and known conditions to calculate the ALR metric. Thus, a metric that is sensitive, easily interpreted, and useable is needed for scientist in other fields and ultimately decision makers (Fig. 9).

Now that the model of the ALR metric is developed and tested, it can be applied to new data immediately. The base satellite data are continuously collected and processed for the public use. There is a benefit to the no cost and availability of these data when modeling trends. As a time sequence of maps is assembled, trends in these statistics will become available.

5. Conclusions

The use of an all-sky measure of anthropogenic sky glow provides a more realistic estimate of visual sky quality, and such measures are more appropriate to protected areas far from large cities than zenith measurements only. The metric ALR is a deviation from natural metric and as such provides resource managers a method to evaluate the effects within a known framework.

Natural resource managers are interested in the effectiveness of current practices and the need for up-to-date monitoring is essential for adaptive management. Monthly cloud-free composites from the VIIRS DNB may be effectively used to derive all-sky predictions for cloud-free low aerosol conditions. Individual observing sites as well as landscape scale patterns may be followed by generating a series of predictions from each monthly cloud-free composite. With these, it is possible to provide managers with timely metrics for decisions about management practices.

The ability to create timely modeled data is a strength of this simplified model of all-sky light pollution ratios. This work combines physical modeling, remote sensing, and ground-based photometry of night sky brightness to produce a high confidence semi-empirical model.

Acknowledgments

We acknowledge and thank Simon Balm, Ashley Pipkin, Robert Meadows, Bill Wren, Jeremy White and Li-Wei Hung who collected much of the ground based data with the CCD camera. Chadwick Moore provided valuable direction on the objectives and methods of this work. A belated acknowledgement to David Theobald who years ago shared the neighborhood annulus method on equal area projection idea with Dan Duriscoe. The authors also thank the two anonymous reviewers whose work greatly improved the manuscript.

Supplementary materials

Supplementary material associated with this article can be found, in the online version, at doi:10.1016/j.jqsrt.2018.04.028.

References

[1] Krisciunas K. Optical night-sky brightness at Mauna Kea over the course of a complete sunspot cycle. Publ Astron Soc Pac 1997;109:1181. doi:10.1086/133993.
[2] Patat F. The dancing sky: 6 years of night-sky observations at Cerro Paranal. Astron Astrophys 2008;481:575–91. doi:10.1051/0004-6361:20079279.
[3] Pun CSJ, So CW. Night-sky brightness monitoring in Hong Kong: a city-wide light pollution assessment. Environ Monit Assess 2012;184:2537–57. doi:10.1007/s10661-011-2136-1.
[4] Zamorano J, Nievas M, Tapia C, García C, Sanchez de Miguel A, Pascual S, et al. Low-cost photometers and open source software for light pollution research. IAU Gen Assem XXIX 2015. http://www.noao.edu/education/files/Zamorano_IAU2015_LowCost_LP.pdf (accessed January 10, 2016).
[5] Bará S. Anthropogenic disruption of the night sky darkness in urban and rural areas. R Soc Open Sci 2016:3.
[6] Duriscoe DM. Measuring anthropogenic sky glow using a natural sky brightness model. Publ Astron Soc Pac 2013;125:1370–82. doi:10.1086/673888.
[7] Falchi F, Cinzano P, Duriscoe D, Kyba CCM, Elvidge CD, Baugh K, et al. The new world atlas of artificial night sky brightness. Sci Adv 2016:2.
[8] Duriscoe DM. Photometric indicators of visual night sky quality derived from all-sky brightness maps. J Quant Spectrosc Radiat Transf 2016. doi:10.1016/j.jqsrt.2016.02.022.
[9] Hänel A, Posch T, Ribas SJ, Aubé M, Duriscoe D, Jechow A, et al. Measuring night sky brightness: methods and challenges. J Quant Spectrosc Radiat Transf 2017. doi:10.1016/j.jqsrt.2017.09.008.
[10] Treanor PJ. A simple propagation law for artificial night-sky illumination. Observatory 1973;93:117–20.
[11] Berry RL. Light pollution in Southern Ontario. J R Astron Soc Can 1976;70:97–115.
[12] Pike R. A simple computer model for the growth of light pollution. J R Astron Soc Can 1976;70:116–26.
[13] Walker MF. The effects of urban lighting on the brightness of the night sky. Publ Astron Soc Pac 1977;89:405–9. doi:10.1086/130142.
[14] Albers S, Duriscoe D. Modeling light pollution from population data and implications for National Park Service lands. George Wright Forum 2001;18:56–68. doi:10.2307/43597774.
[15] Netzel H, Netzel P. High resolution map of light pollution over Poland. J Quant Spectrosc Radiat Transf 2016;181:67–73. doi:10.1016/j.jqsrt.2016.03.014.
[16] Garstang RH. Model for artificial night-sky illumination. Publ Astron Soc Pac 1986;98:364. doi:10.1086/131768.
[17] Garstang RH. Night-sky brightness at observatories and sites. Publ Astron Soc Pac 1989;101:306–29. doi:10.1086/132436.
[18] Garstang RH. Dust and light pollution. Publ Astron Soc Pac 1991;103:1109. doi:10.1086/132933.
[19] Cinzano P, Falchi F, Elvidge CD. The first World Atlas of the artificial night sky brightness. Mon Not R Astron Soc 2001;328:689–707. doi:10.1046/j.1365-8711.2001.04882.x.
[20] Cinzano P, Falchi F, Elvidge CD, Baugh KE. The artificial night sky brightness mapped from DMSP Operational Linescan System measurements. Mon Not R Astron Soc 2000;318:641–57. doi:10.1046/j.1365-8711.2000.03562.x.
[21] Elvidge CD, Baugh KE, Zhizhin M, Hsu F-C. Why VIIRS data are superior to DMSP for mapping nighttime lights. Proc Asia Pac Adv Netw 2013;35:62. doi:10.7125/APAN.35.7.
[22] Cinzano P, Falchi F. The propagation of light pollution in the atmosphere. Mon Not R Astron Soc 2013;427:3337–57. doi:10.1111/j.1365-2966.2012.21884.x.
[23] Duriscoe D, Luginbuhl C, Elvidge C. The relation of outdoor lighting characteristics to sky glow from distant cities. Light Res Technol 2014;46:35–49. doi:10.1177/1477153513506729.
[24] Luginbuhl CB, Duriscoe DM, Moore CW, Richman A, Lockwood GW, Davis DR. From the ground up II: Sky glow and near-ground artificial light propagation in Flagstaff, Arizona. Publ Astron Soc Pac 2009;121:204–12. doi:10.1086/597626.
[25] Elvidge C.D., Baugh K., Zhizhin M., Hsu F.C., Ghosh T. VIIRS night-time lights. Int J Remote Sens 2017:1–20. doi:10.1080/01431161.2017.1342050.
[26] Duriscoe DM, Luginbuhl CB, Moore Ca. Measuring night-sky brightness with a Wide-Field CCD Camera. Publ Astron Soc Pac 2007;119:192. doi:10.1086/512069.
[27] Mills S, Miller S. VIIRS Day/Night band—correcting striping and nonuniformity over a very large dynamic range. J Imaging 2016;2:9. doi:10.3390/jimaging2010009.
[28] Miller SD, Straka WC, Yue J, Smith SM, Alexander MJ, Hoffmann L, et al. Upper atmospheric gravity wave details revealed in nightglow satellite imagery. Proc Natl Acad Sci U S Am 2015;112:E6728–35. doi:10.1073/pnas.1508084112.
[29] Luginbuhl CB, Duriscoe DM, Moore CW, Richman A, Lockwood GW, Davis DR. From the ground up II: sky glow and near-ground artificial light propagation in Flagstaff, Arizona. Publ Astron Soc Pac 2009;121:204–12. doi:10.1086/597626.
[30] Hollan J. What is light pollution, and how do we quantify it?. In: Proceedings of the Work Pap Darksky Conference; 2009. p. 1–12. http://amper.ped.muni.cz/light/lp_what_is.pdf(accessed October 28, 2015).

[31] Moore CA, Turina F, White J. Recommended indicators and thresholds of night sky quality for nps state of the park reports. (accessed October 29, 2015) https://irmafiles.nps.gov/reference/holding/476525 .
[32] Luginbuhl CB, Boley Pa, Davis DR. The impact of light source spectral power distribution on sky glow. J Quant Spectrosc Radiat Transf 2014;139:21–6. doi:10.1016/j.jqsrt.2013.12.004.
[33] Levin N, Zhang Q. A global analysis of factors controlling VIIRS nighttime light levels from densely populated areas. Remote Sens Environ 2017;190:366–82. doi:10.1016/J.RSE.2017.01.006.
[34] Cao C, Bai Y. Quantitative analysis of VIIRS DNB nightlight point source for light power estimation and stability monitoring. Remote Sens 2014;6:11915–35. doi:10.3390/rs61211915.
[35] Zhang J, Reid JS, Miller SD, Turk FJ. Strategy for studying nocturnal aerosol optical depth using artificial lights. Int J Remote Sens 2008;29:4599–613. doi:10.1080/01431160802020528.
[36] McHardy TM, Zhang J, Reid JS, Miller SD, Hyer EJ, Kuehn RE. An improved method for retrieving nighttime aerosol optical thickness from the VIIRS Day/Night Band. Atmos Meas Tech 2015;8:4773–83. doi:10.5194/amt-8-4773-2015.
[37] Wang J, Aegerter C, Xu X, Szykman JJ. Potential application of VIIRS Day/Night band for monitoring nighttime surface PM2.5 air quality from space. Atmos Environ 2016;124:55–63. doi:10.1016/J.ATMOSENV.2015.11.013.